Research Article Vol. 28, No. 1 / 6 January 2020 / Optics Express 130
Optics EXPRESS

Impact of circadian tuning on the illuminance and color uniformity of a multichannel luminaire with spatially optimized LED placement

SANUSH KHYLE ABEYSEKERA,[1] VINEETHA KALAVALLY,[1,*] MELANIE OOI,[2] AND YE CHOW KUANG[2]

[1] *Department of Electrical and Computer Systems Engineering, School of Engineering, Monash University Malaysia, Bandar Sunway 47500, Malaysia*
[2] *Faculty of Science and Engineering, University of Waikato, Hamilton 3216, New Zealand*
[*] *vineetha@monash.edu*

Abstract: Potential advantages offered by multichannel luminaires with regards to spectral tuning are frequently overshadowed by its design challenges, a major one being the non-uniformity in illuminance and color distribution. In this paper, we present a formulation using genetic algorithm (GA) to optimize the Light Emitting Diode (LED) placement, yielding 40% superior uniformity in illuminance and color distributions compared to existing analytical formulations, substantially reducing the reliance on optical design for this purpose. It is specifically shown that our approach is employable for circadian tuning applications, even when heavily constrained by industry specifications on panel size and minimum LED separation.

1. Introduction

For more than a century, the only purpose of indoor lighting design was to provide ample illumination to enable human activity. However, the discovery of the significant impact of non-visual effects of light has propelled human-centric lighting design to the forefront of lighting technology research [1–3]. New advances in the field have introduced circadian tunable light to improve employee health and well-being [1,2,4], lighting design to improve mobility and functionality of the visually impaired [5–7], and for medical therapy to control the circadian rhythm of patients [8,9]. While most of the research on luminaires concentrates on the emulation of desired spectral characteristics during illumination, less attention is paid to the physical light quality. In our work, we present a design method to enhance emission characteristics of luminaires by improving both illuminance and color uniformity.

Three methods exist to achieve spectral tunability in luminaires: cycling through white LEDs with different correlated color temperatures (CCT) [10], color mixing monochromatic with white LEDs for better tunability [11], and color mixing exclusively monochromatic LEDs for the highest flexibility in spectral tuning [12–15]. Each method uses multiple LED channels independently driven at pulse width modulated (PWM) duty cycles to control output intensity. The first method of using channels with predominantly broadband white LEDs achieve spectral tunability by selectively activating channels with the required CCT. It limits the ability of the luminaire to perform finer spectral manipulations and mitigates the total emitted output flux as only a single channel becomes active at a time. The hybrid method typically uses a string of monochromatic LEDs with a phosphor-converted (PC) white LED to achieve spectral tunability with a finer resolution by color mixing. However, the restricted range of tunability and lower luminous efficacy of PC LEDs limit its application. The exclusively monochromatic approach on the other hand provides the ability to perform finer spectral tuning for a broad range of applications at a higher luminous efficacy. Therefore, the proposed uniformity optimization methods were modelled for a luminaire with purely monochromatic color mixing.

#381115 https://doi.org/10.1364/OE.381115
Journal © 2020 Received 23 Oct 2019; revised 11 Dec 2019; accepted 12 Dec 2019; published 23 Dec 2019

Optics EXPRESS

Existing literature presents three methods to maximize physical color quality: illumination correction through free-form lens design [16–18], numerical layout optimization for LED placement [19–21], and analytical layout optimization [12,14,22,23]. Freeform lens design for specific illumination applications presents a plethora of complications including difficulties encountered during manufacturing related to injection molding of dies, manufacturing defects, decrease in light control efficiency, and the inability to use economies of scale due to small scale manufacturing. Furthermore, as a single lens may only be used to control the output distribution of a single LED channel at a time, most lens models are irrelevant for color mixing applications.

An alternative approach widely encountered in modern literature is geometrical modelling of LED distributions on the luminaire emission plate to obtain uniform illumination and color-mixing on the illuminated surface. Algorithms for analytical layout optimization originally introduced by Moreno *et al.* propose the use of a specialized adaptation of the Sparrow's criteria [22]. The focus of this method is to optimize the LED separation such that the illuminance distributions from all LEDs merge to form a maximally flat region of illumination at the center of the illuminated surface. However, the intrinsic structure of the analytical formulation exclusively considered the central region of the illuminated surface and thus has poor overall uniformity performance. Furthermore, the rigid nature of the formulation prevents the incorporation of external constraints such as limits on panel diameter and minimum LED separation which are imperative for commercialization.

On the other hand numerical optimization approaches utilize genetic algorithms (GA) [20,21] or the simulated annealing algorithm [19] to calculate optimum LED distributions. Collectively, these algorithms converge towards an optimal solution by randomly assigning LED positions or by modifying a certain aspect of the LED distribution to maximize intensity uniformity on the illuminated surface. The GA proposed in [20] obtains the optimum LED distribution using a fitness function containing illumination uniformity, average illumination at the illuminated surface, and the amount of LEDs used. The proposed algorithm could optimize LED distributions with multiple transmission characteristics provided they belonged to the same color channel. A different approach proposed by [21] uses GA to optimize LED coordinates on a spherical surface and introduces lateral displacement to the optimization problem. High illumination uniformity for individual LED channels are achieved by increasing LED density. But these arrangements compromise on production cost and the lack of spatial freedom in high density environments limit the uniformity achievable for higher number of color channels.

Despite the remarkable performance of existing uniformity optimization methods, they predominantly support single channel optimization. Existing work on multichannel optimization address specific design criteria with limited generalizability. This paper proposes an optimization formulation for a multichannel luminaire to obtain LED placement with high illumination and color uniformity. The ability of optical radiation to stimulate the melanopsin photoreceptor that can contribute to the non-visual effects of light in humans, described as Melanopic Efficacy of Luminous Radiation (MELR) recently by CIE [24] has been used to represent the circadian impact of the luminaire.

Two possible combinations of LEDs with wide circadian tunability is analyzed and the best combination is selected based on the physical light quality. Section 2 details the required theoretical knowledge and the modelling approach. Section 3 illustrates the importance of each optimization step and introduces the physical constraints of the optimization problem. A stochastic procedure to obtain the best LED separation for minimal thermal damage is also presented. Section 4 investigates the performance of the optimized LED panel over a range of MELR values. Optimization results are validated against illuminance distributions obtained by raytracing. Section 5 concludes this paper.

Optics EXPRESS

2. Modelling for optimal illuminance and color uniformity

We start by offering the necessary theoretical background on photometric calculations needed to comprehend the computation of illumination and color uniformity. Subsequently, the objective function, decision variables, and constraints of the optimization algorithm are introduced. Finally, the generalized optimization approach is proposed to maximize uniformity.

2.1. Photometric calculations

Formulations for calculating the illuminance distribution on a target surface by multiple LEDs occupying a parallel surface above it have been a popular topic of discussion [12,16,19,21–23,25]. The corresponding expressions vary from each other depending on the input photometric characteristics driving the discussion. In the scope of this paper, being limited to a rigid LED selection naturally nominates luminous intensity as a suitable starting point for our study. The following section summarizes the necessary derivation needed to calculate the illuminance distribution at the target surface.

Although the emitting surface of a modern LED is enclosed by a protective encapsulating resin and a silicone based aspheric lens, its illumination pattern can be modelled by a near perfect Lambertian emitter. Therefore for practical applications, the illuminance distribution E_θ can be modelled by a cosine function of the viewing angle θ [22].

$$E_\theta = E\cos^m\theta \tag{1}$$

Here, E is the illuminance measured perpendicular to the LED and the magnitude of m depends on the viewing angle at half power $\theta_{1/2}$ [22].

$$m = \frac{-\ln(2)}{\ln(\cos^{-1}\theta_{1/2})} \tag{2}$$

Figure 1 illustrates the geometric interpretation of the illuminance level on the target surface at point C due to an LED at point A on the panel surface. The expression for $\cos\theta$ in Eq. (3) can be easily obtained using vector algebra and the cosine rule. Illuminance E at point C due to a single LED E_i can then be expressed by substituting Eqs. (1) and (3) to the cosine law of illumination. The z_i term in Eq. (4) can be omitted for a source distribution on a planar panel surface.

$$\cos\theta = \frac{(z_k - z_i)}{\left[(x_k - x_i)^2 + (y_k - y_i)^2 + {z_k}^2\right]^{1/2}} \tag{3}$$

$$E_i(x_k, y_k, z_k) = \frac{E_i {z_k}^{m+1}}{\left[(x_k - x_i)^2 + (y_k - y_i)^2 + {z_k}^2\right]^{(m+3)/2}} \tag{4}$$

$$E(x_k, y_k, z_k) = \sum_{i=1}^{n} \frac{E_i {z_k}^{m+1}}{\left[(x_k - x_i)^2 + (y_k - y_i)^2 + {z_k}^2\right]^{(m+3)/2}} \tag{5}$$

In extension, the total illuminance at any point (x_k, y_k, z_k) on the target surface due to n LEDs can be calculated by Eq. (5). Illuminance for the i^{th} LED E_i is expressed as a photometric quantity in Lux (lx), however it can also be applied as a radiometric quantity in Wm^{-2} to calculate irradiance without modification. Equation (5) can be applied to a predefined grid of coordinates on the target surface to construct a distribution for the illuminance level, from which the illuminance uniformity can be determined. This paper uses the uniformity formulation proposed by the European Standard EN12464-1 for Indoor Lighting [26] to guide the evaluation of uniformity for the LED panel. The standard proposes a proportion between the average E_{mean} and the minimum E_{min} illuminances where illuminance uniformity $\eta = 1$ in Eq. (6) represents

Optics EXPRESS

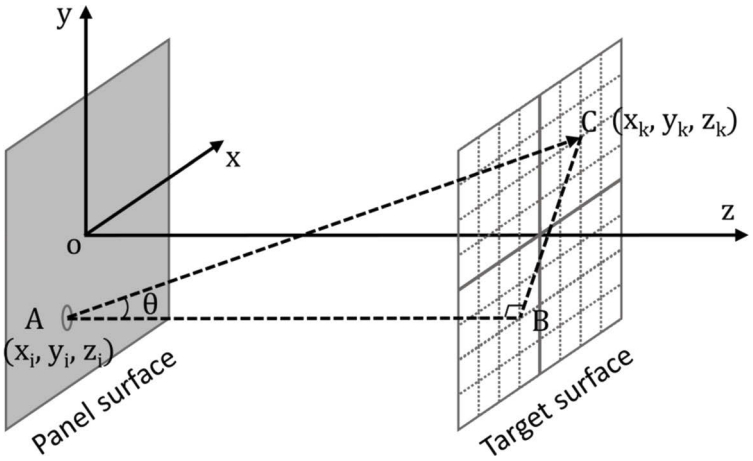

Fig. 1. Schematic diagram for the illuminance at point C on the target illuminated surface resulting from a LED at point A.

perfect uniformity. Additional constraints on the measurement grid d_{grid} in Eq. (7) sets a minimum resolution on the grid where d represents the largest dimension of the target surface. In this paper $d_{\text{grid}} = 2\text{mm}$ for $z_k = 34\text{mm}$ at $d = 8\text{cm}$ and $d_{\text{grid}} = 2\text{cm}$ for $z_k = 1.8\text{m}$ at $d = 1\text{m}$.

$$\eta = \frac{E_{\min}}{E_{\max}} \tag{6}$$

$$d_{grid} = 0.2(5^{\log_{10} d}) \tag{7}$$

In theory, a multispectral illumination source with ideal illuminance uniformity in all spectral bands will produce an output with ideal color uniformity or no color error. However physical constraints on LED placement and the capability of the spatial optimization algorithm to converge to a global optimum sets an upper limit to the maximum attainable uniformity. Therefore, a term to assess color homogeneity is introduced as an optimization objective.

For indoor lighting applications, the difference in the CIE1976 chromaticity space is typically used as a measure of color consistency [12,27]. In contrast to prior chromaticity diagrams, the CIE1976 uniform coordinate system is desirable as it gives an unbiased estimate of color error dependent only on the non-uniformity of the illuminance distribution. It can be expressed as $\Delta u'v'$, the Euclidean distance between a reference color point at the center of the target surface (u_0', v_0') and (u', v') at a desired coordinate (x_k, y_k, z_k) on the same plane.

$$\Delta u'v'(x_k, y_k, z_k) = \sqrt{(u'(x_k, y_k, z_k) - u_0')^2 + (v'(x_k, y_k, z_k) - v_0')^2} \tag{8}$$

$$X(x_k, y_k, z_k) = \int_{\lambda=380}^{780} \left(\sum_{i=1}^{n} F_i(x_k, y_k, z_k) L_i(\lambda) \right) \bar{x}(\lambda) d\lambda \tag{9}$$

$$Y(x_k, y_k, z_k) = \int_{\lambda=380}^{780} \left(\sum_{i=1}^{n} F_i(x_k, y_k, z_k) L_i(\lambda) \right) \bar{y}(\lambda) d\lambda \tag{10}$$

$$Z(x_k, y_k, z_k) = \int_{\lambda=380}^{780} \left(\sum_{i=1}^{n} F_i(x_k, y_k, z_k) L_i(\lambda) \right) \bar{z}(\lambda) d\lambda \tag{11}$$

$$F_i(x_k, y_k, z_k) = \frac{{z_k}^{m+1}}{[(x_k - x_i)^2 + (y_k - y_i)^2 + {z_k}^2]^{(m+3)/2}} \tag{12}$$

Standard formulations in colorimetry can be used to calculate the chromaticity coordinates for Eq. (8) using tristimulus values [28]. At any given point on the target surface, tristimulus

Optics EXPRESS

values can be calculated by Eqs. (9)–(11). These formulations exploit the additive nature of the tristimulus functions to obtain the compounded tristimulus produced by color mixing n LEDs. The aggregate spectral power distribution at any point (x_k, y_k, z_k) is obtained by weighting the spectral power density (SPD) of each LED $L_i(\lambda)$ by a weighing factor F_i specified in Eq. (12), at the target surface corresponding to its relative geometric location. The color matching functions are represented by $(\bar{x}, \bar{y}, \bar{z})$ and all SPDs are bounded from $\lambda = 380$nm - 780nm.

2.2. Optimization constraints

Selection of commercial LED combinations with optimal spectral configuration for high light quality and efficient circadian tuning is outside the scope of this paper and will be explored in an accompanying publication. LED emission characteristics of two such combinations, A and B with 4 and 5 channels respectively, that allow wide circadian tunability with high quality and luminous efficacy is depicted in Table 1. The spatial optimization procedure proposed in this paper is tested for both combinations. During this entire optimization procedure, LEDs belonging to the same bin is assumed to have identical spectral performance. The objective function of the proposed optimization maximizes illuminance and color uniformity on the illuminated target surface.

Table 1. Emission characteristics of LED combinations A and B.

Combination ID	Wavelength peak λ_p (nm)	VAHP $\theta_{1/2}$ (degrees)	FWHM σ (nm)	Luminous flux ϕ_v (lm)	Radiant flux ϕ_e (mW)	Number of LEDs n
A	455	150	20	23	647	2
A	530	125	30	102	183	6
A	590	125	20	56	109	8
A	634	80	16	43	272	4
B	460	150	20	38	877	2
B	530	125	30	118	211	5
B	590	125	20	56	109	8
B	627	125	20	64	307	3
B	634	80	20	43	268	3

VAHP: viewing angle at half power, FWHM: full width at half maximum.

Optical requirements adapted from European Standard EN 12464-1 specify a suitable optimization target for illuminance uniformity as a minimum of 0.8 to guide the arrangement of multiple luminaire units in an indoor environment. The same criteria can be used to model the LED distribution of an individual luminaire without the loss of generalizability. LED panel dimensions were determined after considering power requirements, LED driver capacity, and heat sink efficiency. Table 2 illustrates all mechanical and optical specifications governing the LED panel optimization.

All modelling is performed to optimize illuminance distributions generated at the diffraction surface rather than at the illuminated surface of the luminaire preventing convergence to suboptimal solutions. At the illuminated surface, the higher elevations make the relative distance between LEDs negligible, thus approximating the entire LED panel as a singular point source. It hinders the ability of the optimization algorithm to clearly perceive the optimization direction. For brevity, not all modelling results are shown for both combinations A and B.

2.3. Optimization approach

The spatial optimization problem discussed in this paper can be interpreted as a metaheuristic, where an optimization algorithm finds the optimal solution for an LED distribution among an

Optics EXPRESS

Table 2. Mechanical and optical specifications constraining the LED panel optimization.

Specification	Bound
LED panel diameter	80mm
Elevation between panel and diffractive surface	64mm
Diffractive surface diameter	80mm
Illuminated surface diameter	1000mm
Elevation between panel and illuminated surface[a]	1800mm
Illumination uniformity requirement[a]	≥0.8

[a]Based on European Standard EN 12464-1.

infinitely large solution space. Selecting a suitable combination of optimization algorithm and objective function pair will improve the likelihood of achieving a global optimum and thus increase the repeatability and reproducibility of the optimization result. Furthermore, restrictions on maximum LED panel size and minimum LED separation requires the proposed algorithm to be able to constrain the optimization output to a subset of solutions.

Genetic algorithms (GA) are a popular form of evolutionary optimization algorithms that perform very well on solution space search problems [29,30]. Traditional GAs are based on Darwin's Theory of natural selection, survival of the fittest. GAs are initialized by a randomly generated population of solutions commonly known as chromosomes. Each chromosome is evaluated by an objective function that evaluates its fitness. Chromosomes with higher fitness values are given a higher probability for being selected to mate. Successful chromosomes crossover and create the next generation of solutions. Random mutations are introduced to prevent convergence to local optimum. As generations progress, the solution becomes biased towards chromosomes with higher fitness values. The solution converges to a global optimum after several iterations.

In the spatial optimization problem addressed here, each LED represents an individual decision variable. The optimization processes of early GAs progressed independently of the structure of the chromosome, thus were incapable of segregating individual variables within the same chromosome introduced from multi-objective optimization problems. This paper uses a controlled elitist genetic algorithm (CEGA), a form of multi-objective optimization algorithm that considers each LED as a distinct dimension [31]. The optimization procedure is illustrated in Fig. 2.

The algorithm is initialized by defining emission characteristics for LEDs belonging to N channels, minimum number of LEDs n_i required by each channel i, and the optimization constraints. The European Standard EN 12464-1 recommends a vertical distance of $z_k = 1.8$m between the LED panel and the illuminated surface. However at higher elevations, apparent illuminance uniformity given by Eq. (6) increases irrespective of LED placement due to a significant drop in overall illuminance level. Consequently, modelling was performed for illuminance distributions generated at the diffusion surface of the luminaire at $z_k = 34$cm. CEGA treats all variables within the chromosome independently. Thus, grouping of LEDs within the chromosome corresponding to color channels is not possible. LED channels were optimized individually, starting from the LED channel with the highest number of minimum LEDs. A global variable was defined to store Cartesian coordinates of the optimized LEDs. A subroutine created within the CEGA algorithm enforces the minimum separation between LEDs at each generation.

$$\Psi = \vee\Delta u'v' - \eta \tag{13}$$

Fitness of each individual chromosome is calculated by minimizing the objective function in Eq. (13). The first term considers the color where $\vee\Delta u'v'$ is the maximum error with respect to the center of the target surface and the second term yields illuminance uniformity at the target

Optics EXPRESS

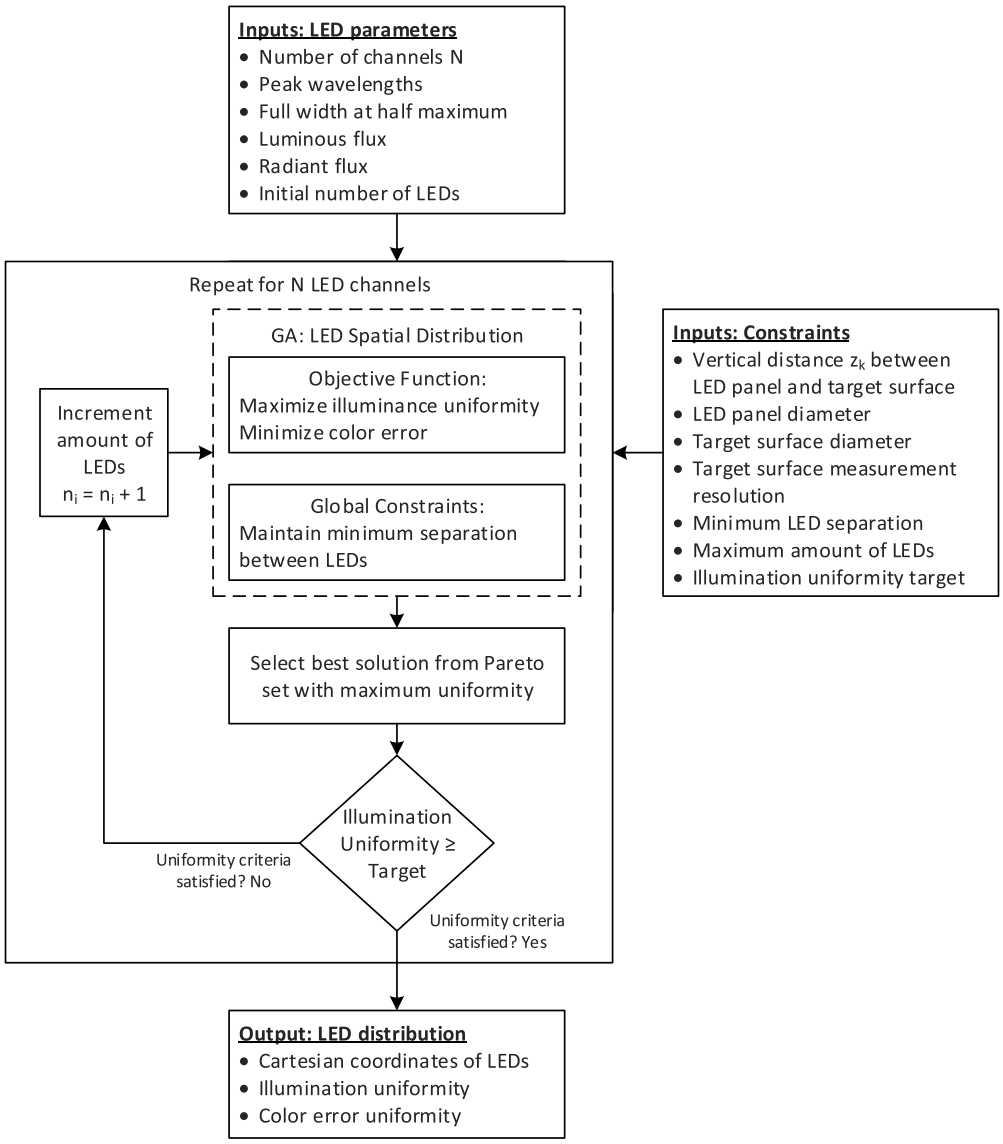

Fig. 2. Algorithmic flow of the optimization procedure. If the target uniformity is not achieved within 10 iterations, the GA iteration with maximum uniformity will be used as the optimum LED distribution.

surface. The uniformity term only considers the LEDs belonging to the current channel and the color error term includes the LEDs stored within the global variable. Within individual channels, the localized CEGA prioritizes achieving higher uniformity as the fitness function subsidizes uniformity by a higher degree. In contrast, the color error term drives the global optimization process between multiple channels to improve color mixing performance by guiding the relative arrangement of all LED channels.

The solution with the highest uniformity from the output Pareto set is selected as the final LED distribution for the current channel. If the uniformity falls below the target uniformity of $\eta = 0.8$, the number of LEDs are increased by 1 and the GA repeated. If the uniformity does not equal to

Optics EXPRESS

or exceed 0.8 after 10 iterations, LED distribution with the highest uniformity is selected as the output.

3. Performance characterization of the optimization algorithm and constraints

This section validates the proposed optimization procedure by analyzing the enhancements to illuminance and color uniformity achieved by each component of the optimization procedure. Subsequently, the effects on the minimum separation between LEDs are considered. A compromise is made to increase separation while maintaining sufficient uniformity to improve thermal performance.

3.1. Evaluation of optimization approach

The performance of the optimized LED distributions for combination B generated by four optimization algorithms are analyzed in Table 3. Each subsequent algorithm is achieved by augmenting the optimization procedure until the fully realized form presented in this paper is reached in algorithm 4. Figure 3 illustrates the corresponding illuminance distributions at the diffusion surface.

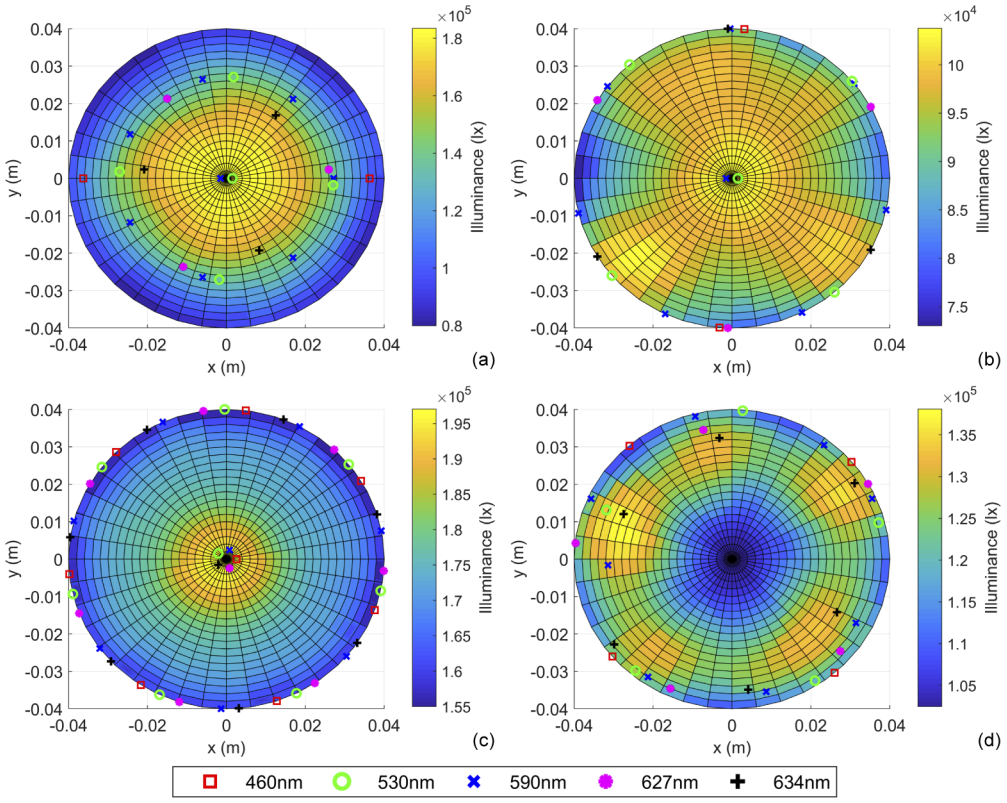

Fig. 3. Illuminance distribution at target surface for combination B. (a) Algorithm 1 (analytical), (b) Algorithm 2, (c) Algorithm 3, and (d) Algorithm 4 (proposed). The markers indicate the spatial arrangement of individual LEDs. All LEDs are driven at rated current.

Algorithm 1 emulates the analytical intensity uniformity formulation proposed by Moreno *et al.* [22] where the total number of LEDs remain unchanged at 21. Channels with less than 4 LEDs are arranged in a circular configuration. Remaining channels are arranged in a circular configuration with a single centric LED. Centric LEDs are marginally offset from the geometric origin of

Optics EXPRESS

Table 3. Performance characterization of four optimization algorithms for combination B.

Description	Algorithm 1	Algorithm 2	Algorithm 3	Algorithm 4
Optimization type	Analytical	Numerical	Numerical	Numerical
Constraint on LEDs	Fixed	Fixed	Variable	Variable
Distribution radius	Fixed	Fixed	Fixed	Independent
Required η	Not applicable	Not applicable	>0.800	>0.800
Number of LEDs	21	21	40	28
Achieved η	0.458	0.579	0.831	0.862
Achieved $\vee\Delta u'v'$	0.037	0.145	0.016	0.038

the panel surface to prevent overlap. A special adaptation of Sparrow's criteria calculates the analytical radius for the LED distribution of each channel. An explicit expression for illuminance distribution $E_{sp}(x_k, y_k, z_k)$ for each configuration can be derived by extending (5). Differentiating $E_{sp}(x_k, y_k, z_k)$ twice and setting $\partial^2 E_{sp}(x_k, y_k, z_k) / \partial x^2 = 0$ at $x = 0$ and $y = 0$ yields a unique analytical expression for uniformity of each channel configuration [22]. Figure 3(a) shows that this preliminary formulation creates a maximally flat region of illumination at the center of the target surface at the expense of illuminance uniformity at the perimeter. The resulting distribution indicates poor uniformity performance.

Algorithm 2 replaces Sparrow's criteria with CEGA to numerically calculate optimal radius. Individual channels are constrained to a common radius. Compared to the previous stage, illuminance uniformity shows a considerable improvement. Figure 3(b) indicates channels with a centric LED being driven to the perimeter of the panel, thus improving overall uniformity. However, the simple numerical optimization algorithm used here does not account for color uniformity. Therefore, intensity uniformity of each individual channel is improved at the cost of color uniformity which relies on the uniform interaction of all LED channels.

In algorithm 3, the optimization procedure is given the ability to increase the number of LEDs to achieve a target uniformity of 0.8. The illuminance uniformity approximately equals the unimpaired CEGA algorithm with the added cost of an immense increase in the number of LEDs. However, excess LEDs yield the lowest color error. Algorithm 4 optimizes each LED with an independent radius and the resulting configuration achieves the highest illuminance uniformity with the best LED economy. The illuminance range is similar to that generated by the other algorithms, but with a slightly reduced illuminance at the center of the target surface.

The four algorithms presented here illustrate that the use of the proposed optimization formulation considerably improves both the illuminance uniformity and the color error. The low standard deviation achieved for repeated experiments presented in Table 4 indicates a high rate of convergence.

Table 4. Simulated panel performance against lower limits of LED separation.

Minimum separation δ (mm)	Combination A			Combination B		
	Uniformity η ($x10^{-2}$)	$\vee\Delta u'v'$ ($x10^{-2}$)	Number of LEDs	Uniformity η ($x10^{-2}$)	$\vee\Delta u'v'$ ($x10^{-2}$)	Number of LEDs
3	86.0 ± 0	2.6 ± 0	24 ± 0	86.0 ± 5	3.9 ± 0.1	27 ± 1
4	86.1 ± 5	3.9 ± 0.3	24 ± 0	83.9 ± 3	5.0 ± 0.3	28 ± 1
5	85.9 ± 3	3.5 ± 0.4	24 ± 1	84.1 ± 0	4.9 ± 0	28 ± 0
6	85.5 ± 1	3.9 ± 0.1	25 ± 1	84.2 ± 6	5.4 ± 0.3	31 ± 2
7	86.0 ± 9	4.7 ± 0.8	27 ± 3	84.5 ± 0	4.7 ± 0	37 ± 0
8	82.6 ± 8	4.8 ± 1.5	27 ± 0	78.0 ± 4	7.7 ± 1.0	33 ± 3

Optics EXPRESS

3.2. Effects of minimum LED separation

High power LEDs used in most modern illumination systems generate an excessive amount of parasitic heat, inducing thermal stress on internal LED components. Changes in junction temperature lead to considerable shifts in emission characteristics compared to specifications. Reducing the total amount of heat generated by the LED panel is out of the scope of this paper. However, heat density can be reduced by modelling for increased LED separation promoting faster heat dissipation and lower localized thermal damage. The optimization algorithm repeated for multiple values of minimum LED separation δ is summarized in Table 4.

$$\delta_j{}' = rank(\delta_j) + rank(\eta_j) + rank(\vee \Delta u'v'_j) + rank(n_j) \tag{14}$$

Each entry in Table 4 denotes the mean and the standard deviation of each channel obtained after 10 repetitions of the optimization algorithm indicating convergence to a global optimum. The upper and lower limits of δ are subsequently governed by the convergence of the algorithm to uniformity values beyond 0.8 and the LED package dimensions. Best δ was selected by a rank order system. Each component in the table was ranked with a positive integer representing its merit. Components with higher merit was assigned higher integers. Ranks for each individual separation j were linearly summed according to Eq. (14). LED separation δ_j with the highest cumulative rank δ_j' was selected as the optimal separation. Highest cumulative rank was achieved by $\delta = 7$mm for both LED combinations.

The uniformity performance of each individual channel at $\delta = 7$mm for combination B is illustrated in Table 5. It reveals that channel 1 fails to individually achieve sufficient uniformity. As an adverse effect at higher δ, more channels indicate performance deficiencies caused by the inability of CEGA to converge to the uniformity target without violating constraints on LED separation. However, enforcing the uniformity target solely on overall uniformity enables us to consider higher δ with performance deficiencies in each individual channel. The final section proposes a testing mechanism to characterize the performance of the LED distribution at different circadian action settings.

Table 5. Performance of individual channels of combination B at rated current.[a]

Channel number	Wavelength peak (nm) λ_p	Uniformity (x10^{-2}) η	Optimized number of LEDs
Channel 1	460	77.9	11
Channel 2	530	87.8	05
Channel 3	590	90.5	08
Channel 4	627	84.9	06
Channel 5	634	81.2	07
Total		84.5	37

[a]Results at diffusion surface $z_k = 34$ mm, $\delta = 7$ mm.

4. Impact of circadian tuning

This section characterizes the performance of the optimized LED distribution based on illuminance uniformity and color error at multiple Melanopic Efficacy of Luminous Radiation (MELR) values. A desired MELR value can be realized by generating a pre-defined spectral mixture of the LED channels. Unless otherwise mentioned, simulations are primarily performed for a target surface elevation of $z_k = 1.8$m as the uniformity of the light distribution is judged at the illuminated work surface. We start by introducing a formulation to generate LED intensity values based on specific MELRs. Subsequently, the best LED combination from Table 1 is selected based on uniformity performance. The following section more rigorously characterizes panel performance

Optics EXPRESS

over a range of MELRs. A subset of three MELR values are used to illustrate finer variations in illuminance distributions against raytracing simulations.

4.1. MELR based LED intensity generation

We propose a formulation to approximate white light with a desired MELR through color mixing for performance characterization of the LED panel. For a SPD $\phi_e(\lambda)$, the MELR expressed by Eq. (15) is defined as the ratio between the melanopic irradiance and illuminance [24]. Here $S_{mel}(\lambda)$ and $V(\lambda)$ represent the melanopic action spectrum and the photopic sensitivity function respectively. For N color channels with n_i LEDs in the i^{th} channel, the additive nature of the radiant flux can be exploited to achieve the total weighted SPD $\phi_e(\lambda)$ by the addition of spectral outputs $\phi_i(\lambda)$ produced by each LED Eq. (16) with T_i weights. Optimal intensity weights T_i required to reproduce the desired MELR can be obtained by numerically solving the restructured MELR expression Eq. (17) subjected to the D_{uv} constraint. D_{uv} is defined as the distance and direction of color shift from the Planckian locus. Given a desired MELR, the proposed expression generates intensity values to approximate light spectra that satisfies the intended MELR constrained within $D_{uv} < 0.0054$ of the Planckian locus [32].

$$MELR = \frac{\int \phi_e(\lambda) S_{mel}(\lambda) d\lambda}{683 \int \phi_e(\lambda) V(\lambda) d\lambda} \tag{15}$$

$$\phi_e(\lambda) = \sum_{i=1}^{N} T_i n_i \varphi_i(\lambda) \tag{16}$$

$$\sum_{i=1}^{N} T_i \{n_i \phi_i(\lambda)[MELR^* 683^* V(\lambda) - S_{mel}(\lambda)] d\lambda\} = 0 \text{ subject to } D_{uv} < 0.0054 \tag{17}$$

The intensity weights T_i produced by Eq. 17 indicates the SPD required to obtain a specific MELR at the LED panel surface. However, the inherent structure of the formulation disregards the relative displacement between LEDs leading to irregular color reconstruction at the target surface. For a target surface elevation z_k known a-priori, initial T_i obtained from Eq. (17) are reweighted such that the desired SPD is achieved at the target surface. Small changes to T_i are made depending on the extent of dispersion for each LED channel.

4.2. MELR based performance characterization

The optimized LED distribution is expected to reproduce output spectra with significant uniformity for any LED intensity combination. The best LED channel combination from Table 1 can now be selected by assessing the average illuminance uniformity and color error for a broad range of MELR values.

Figures 4(a) and 4(b) illustrates the performance of LED combinations corresponding to MELR values from 0.35 to 1.55 spanning the most commonly encountered MELR values in artificial lights. The results show superior performance in illuminance uniformity at higher MELR values for both Combinations A and B with 4 and 5 channels respectively. Combination A exhibits a 0.7% variation across the MELR tuning range, as opposed to only 0.3% for Combination B. In both cases, uniformity is within constrained values demonstrating the success of the optimization approach. The color error also exhibits improved performance at high MELR for Combination A, but is maintained with very minor variations across the MELR range for Combination B. However, Combination B indicate consistently better performance in both illuminance uniformity and color error for all MELR values compared to Combination A. This significant lead in performance is caused by the higher number of LEDs required by combination B (37) to converge to an optimal LED configuration compared to Combination A (30) after optimization. It further explains the

Optics EXPRESS

higher illuminance uniformity of both combinations at higher MELR. The short wavelength LED channel (460nm) with the highest number of LEDs has a more significant presence at higher MELR values. It is evident that increased LED density indicates enhanced performance for a uniformity driven optimization approach.

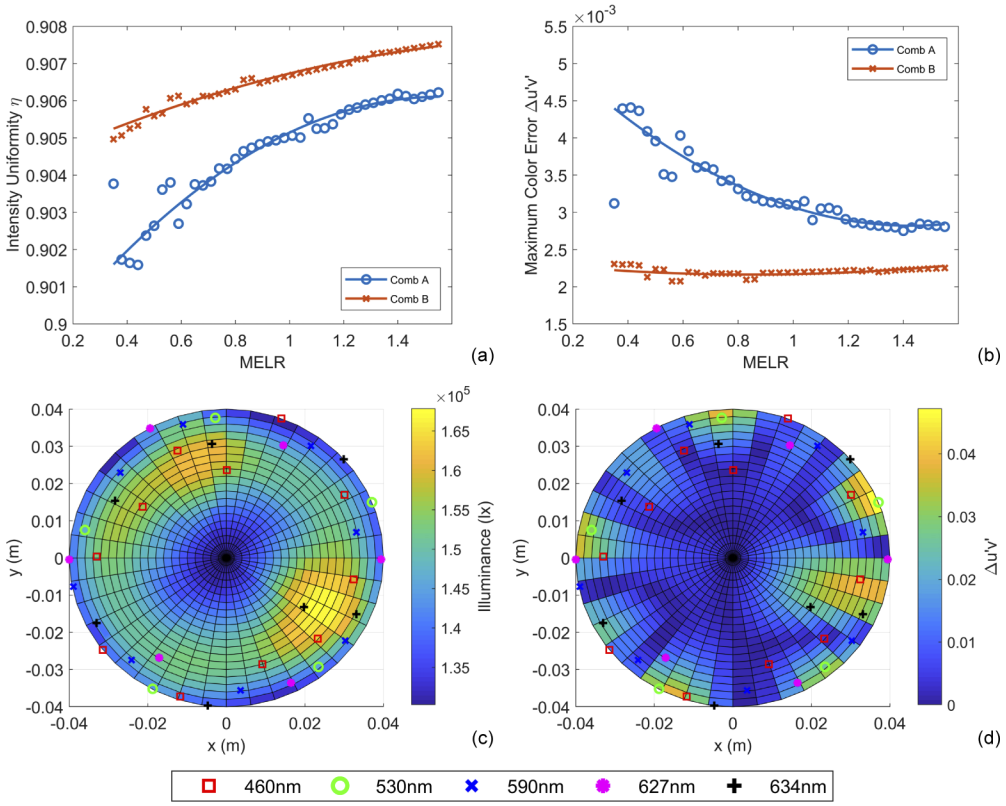

Fig. 4. A comparison of (a) illuminance uniformity and (b) color distribution for combinations A and B. For combination B, (c) and (d) illustrate the illuminance and $\Delta u'v'$ distributions for all channels at rated current, $z_k = 34$ mm, intensity uniformity = 0.845, and $\vee\Delta u'v' = 0.0472$.

Now that that combination B has been identified as the superior alternative, we limit the remainder of our analysis to B. To improve legibility, the overall performance of B with all channels at rated current and its relative LED placement is illustrated in Figs. 4(c) and 4(d). Figure 5(a) illustrates the illuminance contribution of each LED channel required to induce specific MELR values. At higher MELRs, the trend indicates an increased utilization of the less uniform 460nm color channel (Table 5) and a reduced contribution by the longer wavelength (530nm, 590nm, 627nm and 634nm) channels with superior uniformity.

Figure 5(a) indicates that the 530nm channel is consistently driven at rated current while MELR variation is achieved by modifying all remaining channels. As the channel with the highest contribution to luminous efficacy, the 530nm channel remains relevant to the full range of MELRs. On the other hand, as the main channel contributing to high MELR, the 460nm channel with the largest number of LEDs causes the illuminance distribution to improve as seen in Fig. 4(a). The resulting illuminance difference for the entire range of MELRs is shown in Fig. 5(b) to be between 10.05 and 7.42 with better performance at higher MELR. The D_{uv}

Optics EXPRESS

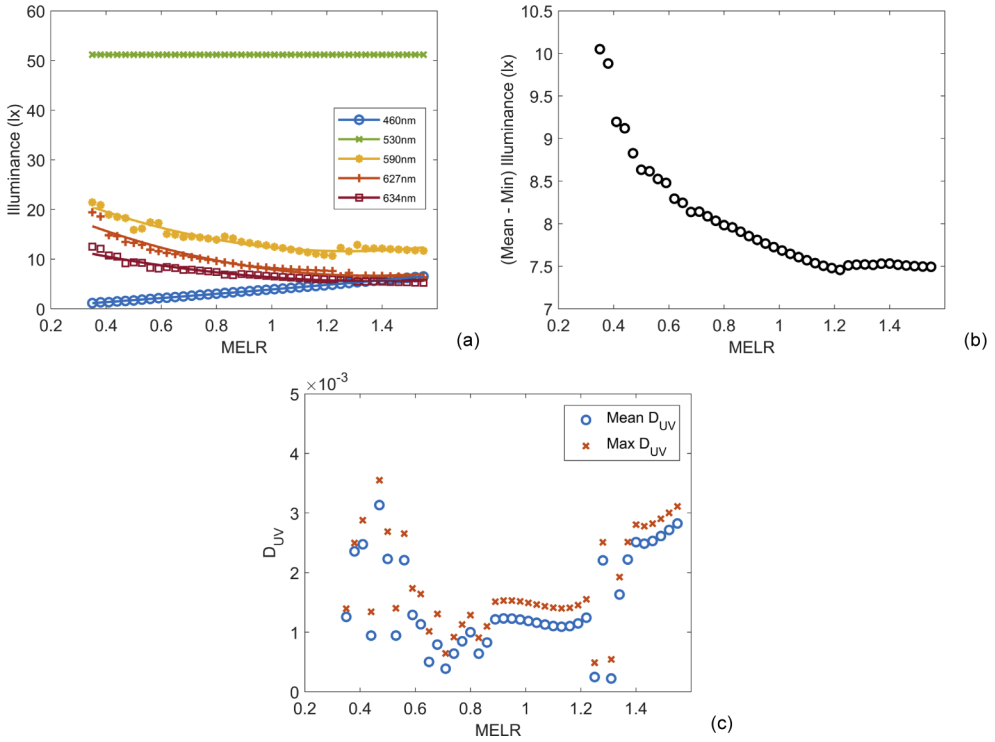

Fig. 5. Performance of combination B (at $z_k = 1.8$ m). Against the target MELR, plot indicate the (a) individual illuminance contribution by each channel with increasing MELR, (b) deviation between mean and minimum illuminance output, and (c) variation in D_{uv}.

characteristics in Fig. 5(c) illustrate that the color distribution of the overall illumination has been maintained within the constrained deviation of 0.0054 from the Planckian locus.

A subset encompassing a range of MELRs, low – 0.45, medium – 0.8, and high – 1.35 were selected for validating the results from theoretically generated illuminance distributions against TracePro simulations using the optimized LED panel. The results are summarized in Table 6. When calculating uniformity of the raytracing results, a crease of 30mm from the perimeter of the illuminated surface was ignored as it does not fairly represent theoretical considerations. Figure 6 illustrates the raytracing simulation for MELR = 0.8.

Table 6. Performance of theoretical vs raytracing illuminance distributions.[a]

Simulation type	Measured performance	MELR = 0.45	MELR = 0.80	MELR = 1.35
Theoretical	Intensity uniformity	0.906	0.906	0.907
Raytracing	Intensity uniformity	0.759	0.739	0.734
Theoretical	Mean illuminance (lx)	94.37	85.20	81.12
Raytracing	Mean illuminance (lx)	68.18	62.01	60.46

[a]Simulation results on illuminated surface at $z_k = 1.8$ m.

Consecutive simulations with increasing number of traced rays show convergence to theoretical simulations with uniformity reaching 0.8. However, hardware restrictions constrained the maximum number of rays traced to 25,000 rays per LED channel. The average illuminance in

Optics EXPRESS

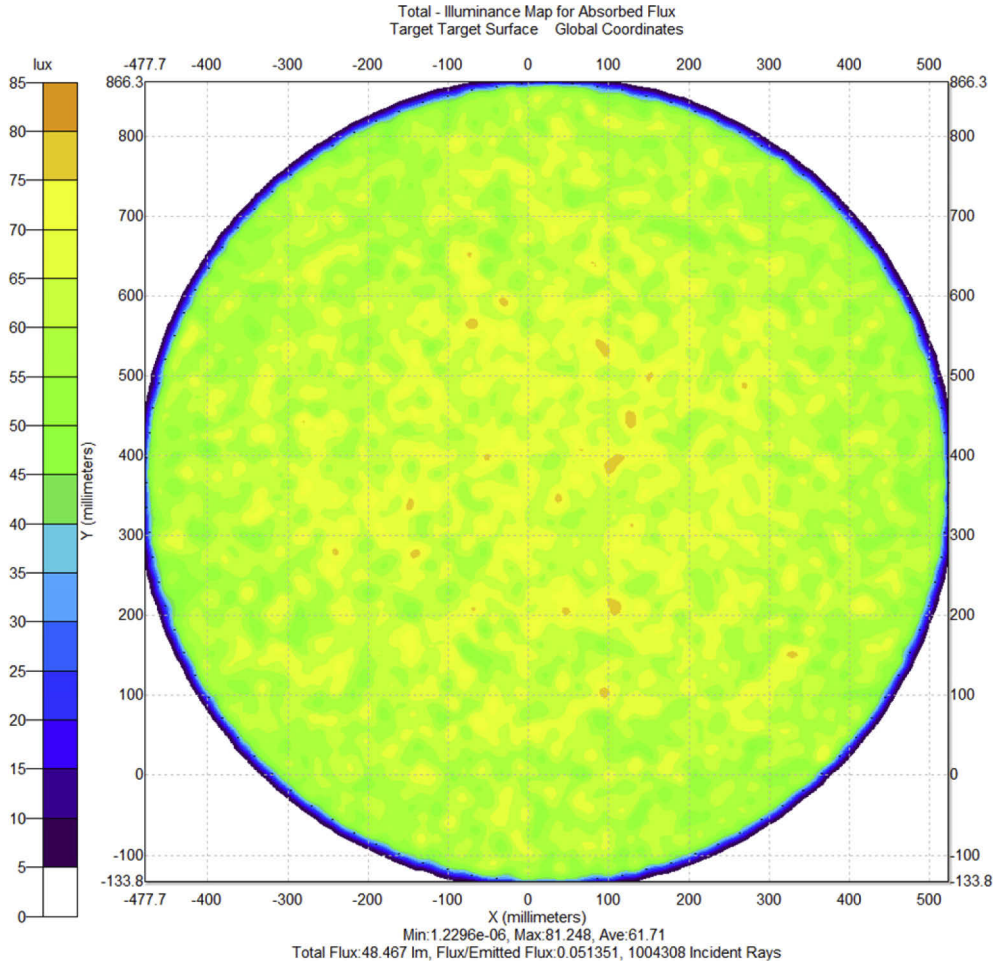

Fig. 6. Illuminance distribution from Raytracing simulations (MELR = 0.8, z_k = 1.8 m). Summary of raytracing output: min flux = 0 lm, max flux = 81 lm, mean flux = 48.5 lm, and incident rays = 1004308.

Table 6 illustrates a 75% similarity between the theoretical and raytracing simulations and an 83% similarity between illuminance uniformities.

5. Conclusion

This study adopts Genetic Algorithms (GA) to perform optimization due to its superiority in obtaining a global solution to multidimensional optimization problems. Using an objective function that constitutes of two terms representing illuminance uniformity and color consistency, LED distributions are optimized at intra and inter-channel levels. Comparison with multiple numerical and analytical methods revealed that the proposed algorithm achieved 40% superior performance with the best LED economy. Repeated trials of the optimization algorithm show convergence to identical solutions with minor standard deviations establishing the stability and accuracy of the optimization model. Physical constraints introduced to the optimization problem closely resemble real manufacturing considerations. The generalizability of the optimization approach was illustrated by achieving an intensity uniformity of 0.8 for two different LED

Optics EXPRESS

combinations with wide circadian tunability. Using Melanopic Efficacy of Luminous Radiation (MELR) as a metric to guide the circadian performance of the panel, it was shown that there exists a tradeoff in illuminance uniformity at higher MELR, with color consistency being maintained within the constrained deviation of 0.0054 from the Planckian locus across the MELR range.

Funding

This study was supported by Collaborative Research in Engineering, Science and Technology (CREST) (grant number P20C1-15/005) and Itramas Corporation Sdn Bhd.

Disclosures

The authors declare no conflicts of interest.

References

1. J. Higuera, W. Hertog, M. Perálvarez, and J. Carreras, "Hybrid smart lighting and climate control system for buildings," in *IET Conference on Future Intelligent Cities*, 2014), 1–5.
2. J. Higuera, W. Hertog, M. Perálvarez, J. Polo, and J. Carreras, "Smart Lighting System ISO/IEC/IEEE 21451 Compatible," IEEE Sens. J. **15**(5), 2595–2602 (2015).
3. I. Chew, D. Karunatilaka, C. P. Tan, and V. Kalavally, "Smart lighting: The way forward? Reviewing the past to shape the future," Ener. Build. **149**, 180–191 (2017).
4. M. L. Amundadottir, S. Rockcastle, M. Sarey Khanie, and M. Andersen, "A human-centric approach to assess daylight in buildings for non-visual health potential, visual interest and gaze behavior," Build. Sci. **113**, 5–21 (2017).
5. M. S. Perlmutter, A. Bhorade, M. Gordon, H. Hollingsworth, J. E. Engsberg, and M. Carolyn Baum, "Home lighting assessment for clients with low vision," Am. J. Occup. Ther. **67**(6), 674–682 (2013).
6. P. Katemake, A. Radsamrong, É. Dinet, C. W. Heng, Y. C. Kuang, V. Kalavally, and A. Trémeau, "Influence of LED-based assistive lighting solutions on the autonomous mobility of low vision people," Build. Sci. **157**, 172–184 (2019).
7. E. Noell-Waggoner, "Lighting and the Elderly," in *Handbook of Advanced Lighting Technology*, R. Karlicek, C.-C. Sun, G. Zissis, and R. Ma, eds. (Springer International Publishing, Cham, 2017), pp. 847–863.
8. C. I. Eastman, M. A. Young, L. F. Fogg, L. Liu, and P. M. Meaden, "Bright Light Treatment of Winter Depression: A Placebo-Controlled Trial," Arch. Gen. Psychiatry **55**(10), 883–889 (1998).
9. A. Shirani and E. K. St Louis, "Illuminating rationale and uses for light therapy," J. Clin. Sleep Med. **5**, 155–163 (2009).
10. M. Bálský, R. Bayer, J. Zálešák, and Z. Panská, "Use of tunable white luminaires for biodynamic lighting," in *2017 18th International Scientific Conference on Electric Power Engineering (EPE)*, 2017), 1–4.
11. N. Trivellin, M. Meneghini, M. Ferretti, D. Barbisan, M. D. Lago, G. Meneghesso, and E. Zanoni, "Effects and exploitation of tunable white light for circadian rhythm and human-centric lighting," in *2015 IEEE 1st International Forum on Research and Technologies for Society and Industry Leveraging a better tomorrow (RTSI)*, 2015), 154–156.
12. I. Moreno and L. M. Molinar, "Color uniformity of the light distribution from several cluster configurations of multicolor LEDs," in *Optics and Photonics 2005*, (SPIE, 2005), 7.
13. T. Wu, Y. Lin, H. Zhu, Z. Guo, L. Zheng, Y. Lu, T.-M. Shih, and Z. Chen, "Multi-function indoor light sources based on light-emitting diodes; A solution for healthy lighting," Opt. Express **24**(21), 24401–24412 (2016).
14. L. L. Zheng, T. Z. Wu, Y. J. Lu, Y. L. Gao, Y. J. Wang, L. H. Zhu, Z. Q. Guo, and Z. Chen, "Spectral Optimization of Three-Primary LEDs by Considering the Circadian Action Factor," IEEE Photonics J. **8**(6), 1–9 (2016).
15. I. Chew, V. Kalavally, C. P. Tan, and J. Parkkinen, "A Spectrally Tunable Smart LED Lighting System With Closed-Loop Control," IEEE Sens. J. **16**(11), 4452–4459 (2016).
16. Z. Qin, K. Wang, F. Chen, X. Luo, and S. Liu, "Analysis of condition for uniform lighting generated by array of light emitting diodes with large view angle," Opt. Express **18**(16), 17460–17476 (2010).
17. A. J. Whang, Y. Chen, and Y. Teng, "Designing Uniform Illumination Systems by Surface-Tailored Lens and Configurations of LED Arrays," J. Disp. Technol. **5**(3), 94–103 (2009).
18. P. Liu, H. Wang, R. Wu, Y. Yang, Y. Zhang, Z. Zheng, H. Li, and X. Liu, "Uniform illumination design by configuration of LEDs and optimization of LED lens for large-scale color-mixing applications," Appl. Opt. **52**(17), 3998–4005 (2013).
19. Z. Su, D. Xue, and Z. Ji, "Designing LED array for uniform illumination distribution by simulated annealing algorithm," Opt. Express **20**(S6), A843–A855 (2012).
20. S. Pal, "Optimization of LED array for uniform illumination over a target plane by evolutionary programming," Appl. Opt. **54**(27), 8221–8227 (2015).
21. Y. Shen and Z. Ji, "Optimizing spherical light-emitting diode array for highly uniform illumination distribution by employing genetic algorithm," J. Photonics Energy **3**(1), 034594 (2013).

Optics EXPRESS

22. I. Moreno, M. Avendaño-Alejo, and R. I. Tzonchev, "Designing light-emitting diode arrays for uniform near-field irradiance," Appl. Opt. **45**(10), 2265–2272 (2006).
23. X. Wang, "LED ring array light source design and uniform illumination properties analysis," Optik **140**, 273–281 (2017).
24. I. C. o. Illumination, "*System for Metrology of Optical Radiation for ipRGC-Influenced Responses to Light*," (International Commission on Illumination, 2018).
25. F.-T. Wu and Q.-L. Huang, "A precise model of LED lighting and its application in uniform illumination system," Optoelectron. Lett. **7**(5), 334–336 (2011).
26. E. C. f. Standardization, "*Light and lighting - Lighting of work places - Part 1: Indoor work places*," (European Standard, Brussels, 2011).
27. "*Solid-State Lighting Technology Fact Sheet*," U. S. D. o. Energy, ed. (United States Department of Energy, 2016).
28. P. J. Alessi, E. C. Carter, M. D. Fairchild, R. W. G. Hunt, C. S. McCamy, B. Kranicz, J. R. Moore, J. H. Nobbs, Y. Ohno, M. R. Pointer, D. C. Rich, A. R. Robertson, J. D. Schanda, R. Seve, P. W. Trezona, K. Witt, and H. Yaguchi, "*Colorimetry*," 978 3 901906 33 6 (International Commission on Illumination, 2004).
29. U. Maulik, "Medical Image Segmentation Using Genetic Algorithms," IEEE Trans. Inform. Technol. Biomed. **13**(2), 166–173 (2009).
30. A. Bajaj and O. P. Sangwan, "A Systematic Literature Review of Test Case Prioritization Using Genetic Algorithms," IEEE Access **7**, 126355–126375 (2019).
31. K. Deb, A. Pratap, S. Agarwal, and T. Meyarivan, "A fast and elitist multiobjective genetic algorithm: NSGA-II," IEEE Trans. Evol. Computat. **6**(2), 182–197 (2002).
32. Y. Ohno, "Practical Use and Calculation of CCT and Duv," Leukos **10**(1), 47–55 (2014).